Supplementary material

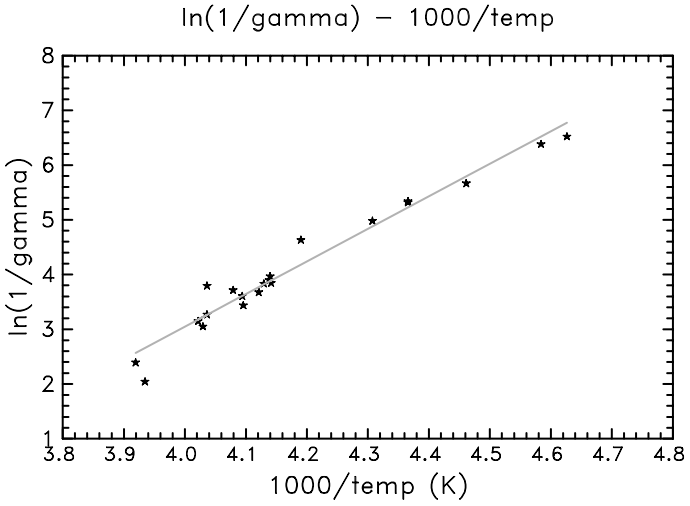

<u>Supplementary Figure S1</u>: Logarithmic representation of γ coefficient in Equation (4) as a function of the site temperature. The stars represent the γ coefficient calculated by the model for each site, the grey line represents a linear regression. Its slope allows evaluation of the activation energy relative to the snow densification mechanism in the model: 49.5 kJ/mol.

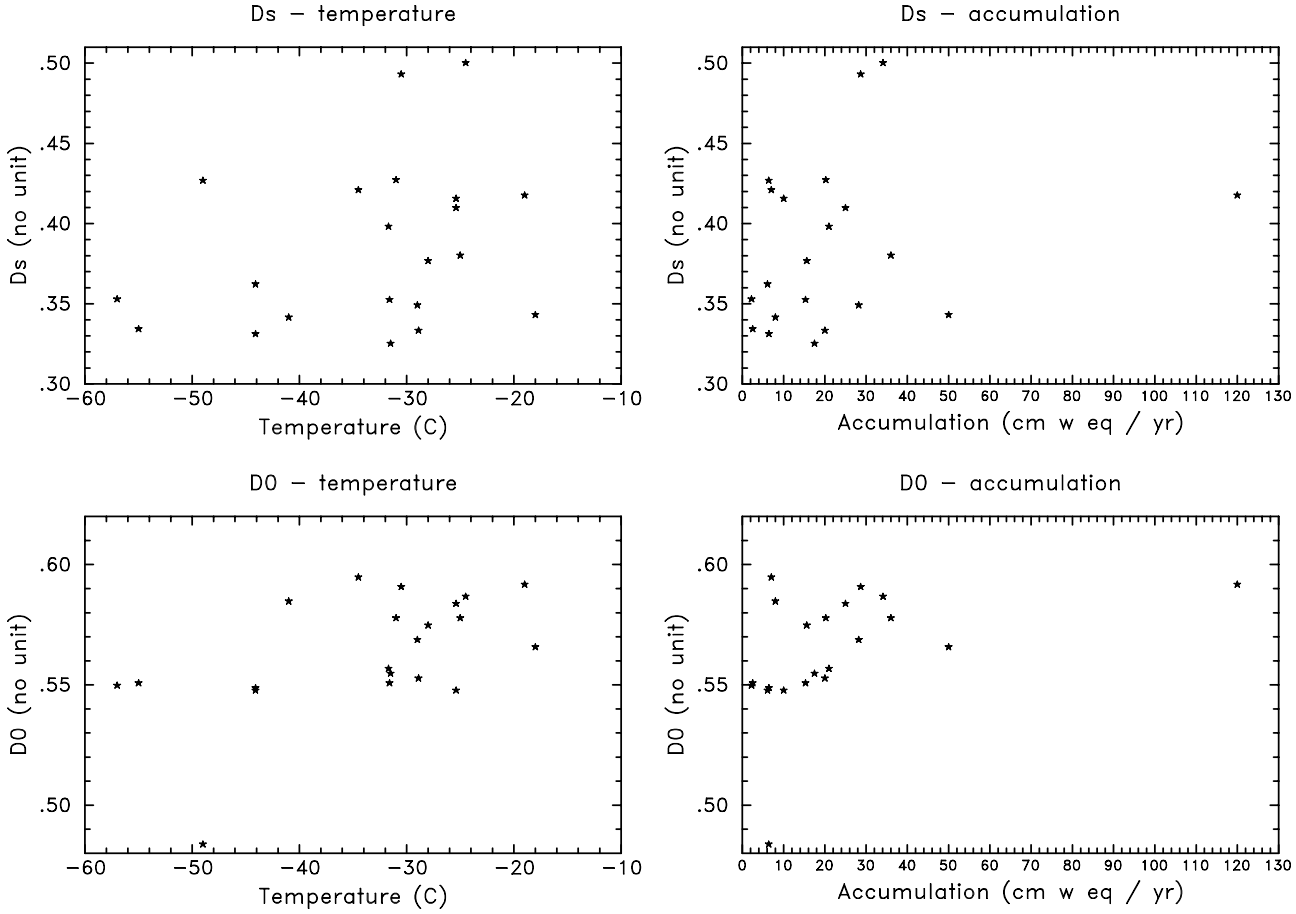

Supplementary Figure S2: Variations of the surface (Ds) and critical (D0) relative densities with site temperature and accumulation. Ds is the value of the polynomial fit to density data represented on Figures S3 and S7 at the surface. D0 is adjusted to minimize the root mean square deviations between model results and the polynomial fit to density data between the surface and the depth at which a density of 840 kg/m^3 is reached. No correlation between Ds or D0 with temperature or accumulation could be found. Although the variability of Ds and D0 are large, their impact on the LID is relatively small as illustrated on Figure S3.

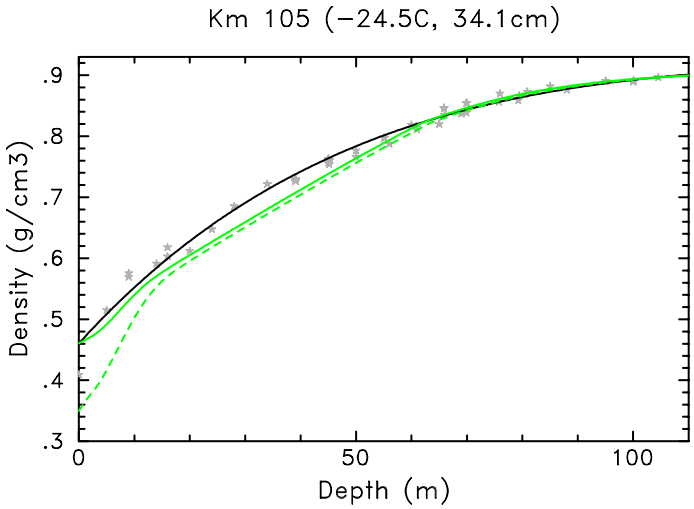

Supplementary Figure S3: Impact of the surface density value (Ds) on model results at Km 105 site. Grey stars represent measured densities, the black line represents a polynomial fit to density data. The two green curves represent model results obtained with two largely different values of the surface density. Lower values of Ds lead to faster modelled densification rates. While the difference between the two densification curves is important at the surface, the two curves are almost similar in the deep firn. The difference on Ds thus does not have much importance for the determination of the LID.

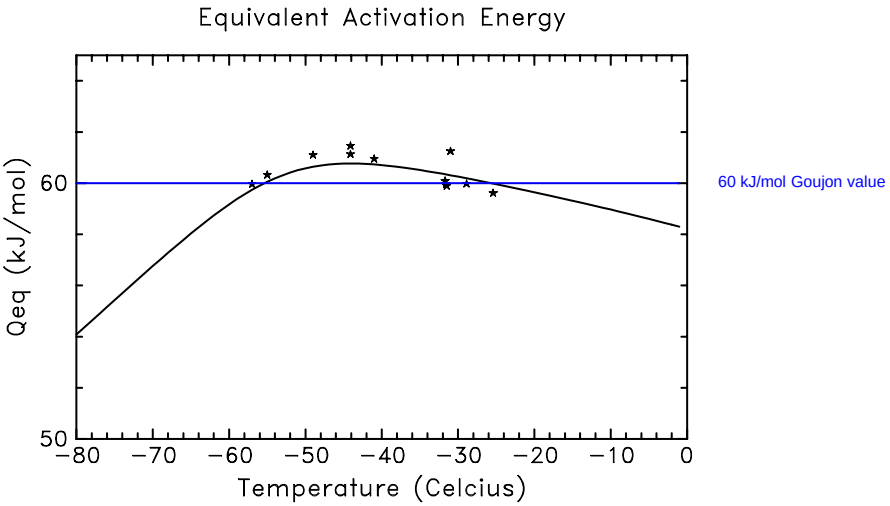

Supplementary Figure S4: Equivalent activation energies calculated for our model (without impurity effect, black line; with impurity effect for present day sites with available calcium concentrations, black stars).The blue line represents the value of 60kJ/mol used in Goujon et al. (2003).

For our model, the equivalent activation energy Q_{eq} is calculated by solving: $e^{\frac{-Q_{eq}}{RT}} = a_1 \times e^{\frac{-Q_1}{RT}} + a_2 \times e^{\frac{-Q_2}{RT}} + a_3 \times e^{\frac{-Q_3}{RT}}$.

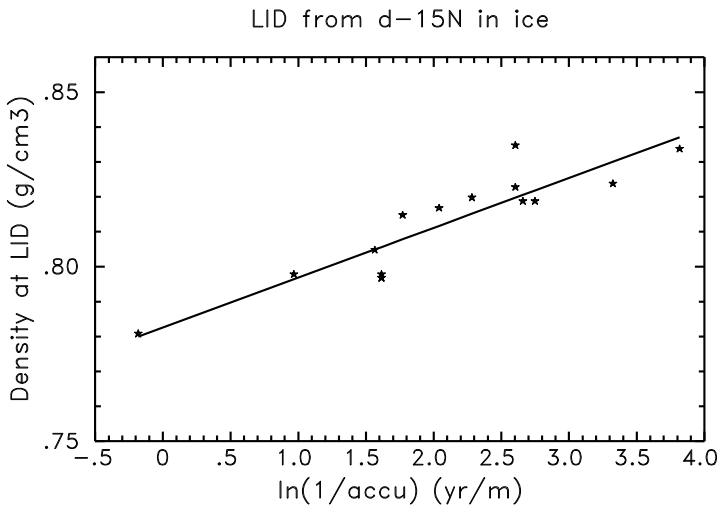

Supplementary Figure S5: Calculated density at LID with the Witrant et al. (2012) model of gas transport in firn (see main text, Section 2.4) as a function of the logarithm of the inverse of the accumulation rate (in m w. eq./yr). The stars show the results at individual firn air pumping sites (12 sites, 15 boreholes), and the line shows the regression presented in Equation (10) of the main text. The correlation coefficient is 0.9.

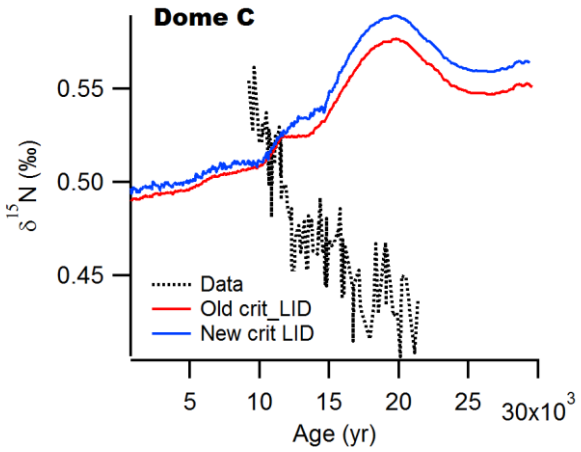

Supplementary Figure S6: Comparison of the measured (in black) and the old modelled $\delta^{15}N$ at Dome C. The simulated $\delta^{15}N$ using the old gas trapping criterion is in red and the simulated $\delta^{15}N$ using the new gas trapping criterion is in blue.

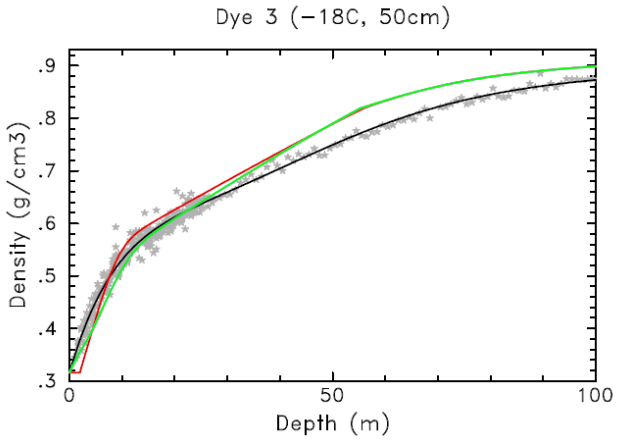
Dye 3 (−18C, 50cm)
Density (g/cm3)
.3
.4
.5
.6
.7
.8
.9
0
50
100
Depth (m)

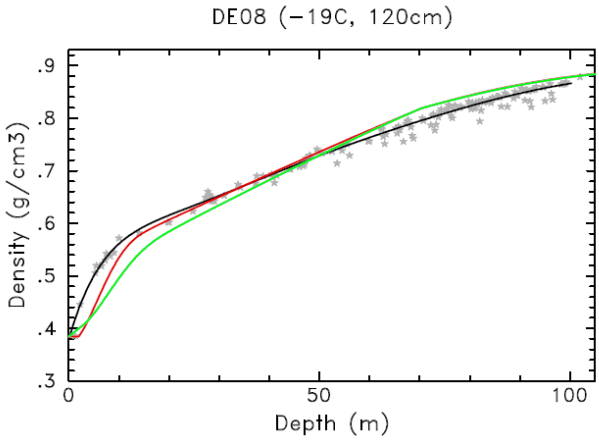
DE08 (−19C, 120cm)
Density (g/cm3)
.3
.4
.5
.6
.7
.8
.9
0
50
100
Depth (m)

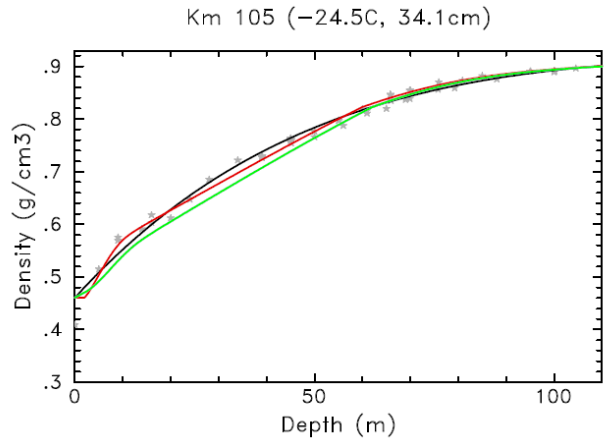
Km 105 (−24.5C, 34.1cm)
Density (g/cm3)
.3
.4
.5
.6
.7
.8
.9
0
50
100
Depth (m)

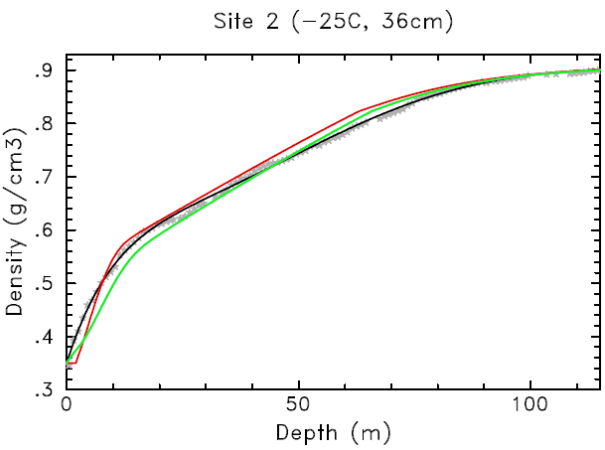
Site 2 (−25C, 36cm)
Density (g/cm3)
.3
.4
.5
.6
.7
.8
.9
0
50
100
Depth (m)

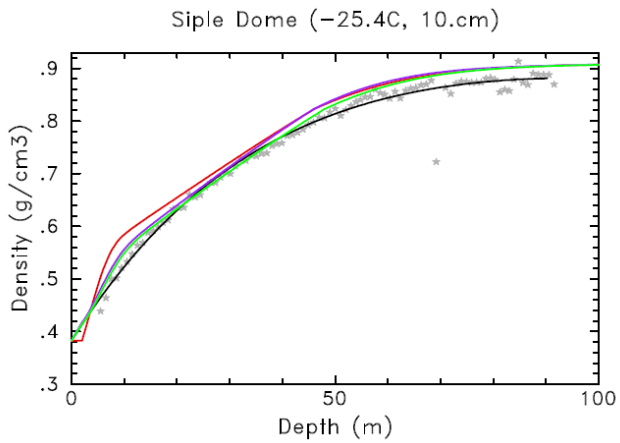
Siple Dome (−25.4C, 10.cm)
Density (g/cm3)
.3
.4
.5
.6
.7
.8
.9
0
50
100
Depth (m)

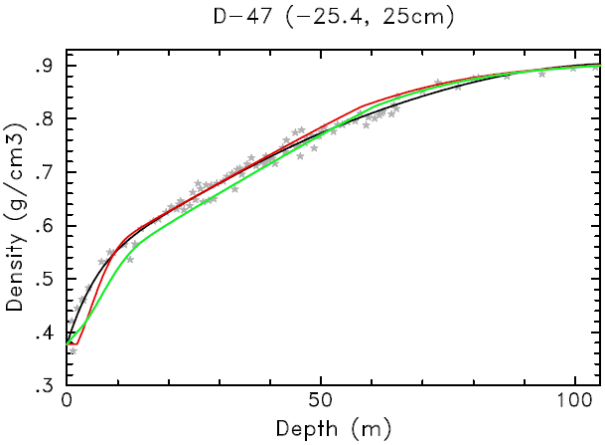
D−47 (−25.4, 25cm)
Density (g/cm3)
.3
.4
.5
.6
.7
.8
.9
0
50
100
Depth (m)

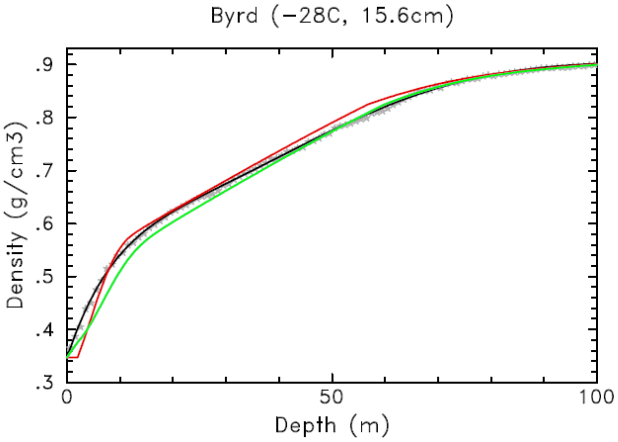
Byrd (−28C, 15.6cm)
Density (g/cm3)
.3
.4
.5
.6
.7
.8
.9
0
50
100
Depth (m)

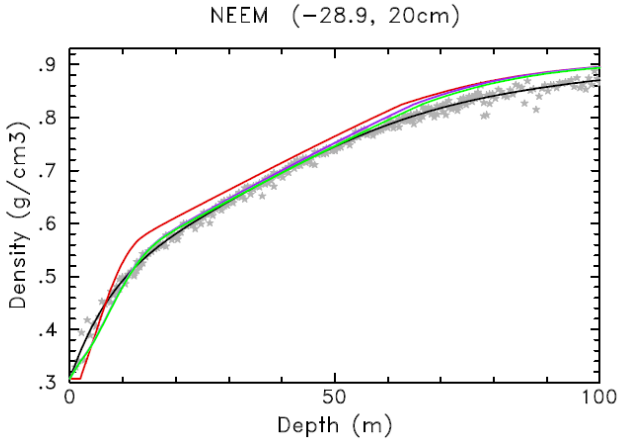
NEEM (−28.9, 20cm)
Density (g/cm3)
.3
.4
.5
.6
.7
.8
.9
0
50
100
Depth (m)

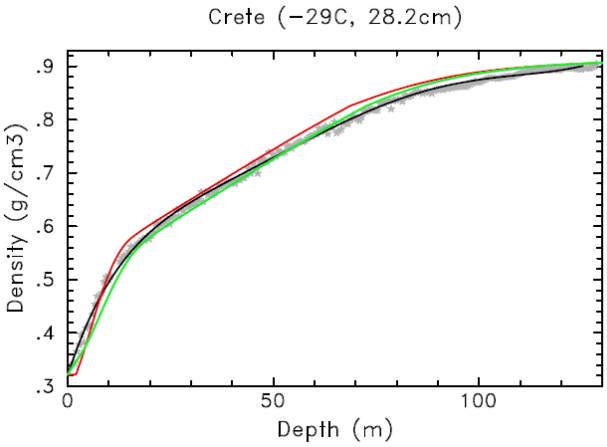
Crete (−29C, 28.2cm)
Density (g/cm3)
.3
.4
.5
.6
.7
.8
.9
0
50
100
Depth (m)

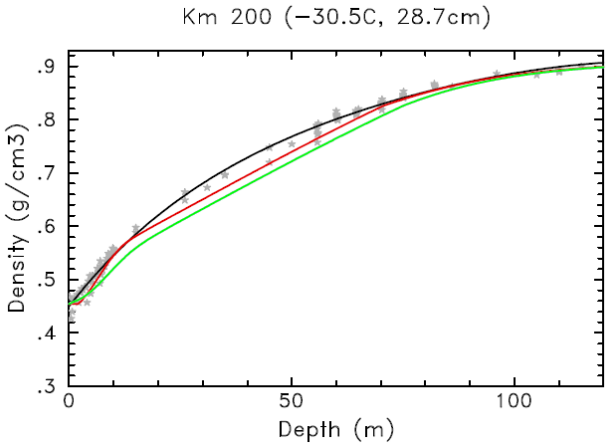
Km 200 (−30.5C, 28.7cm)
Density (g/cm3)
.3
.4
.5
.6
.7
.8
.9
0
50
100
Depth (m)

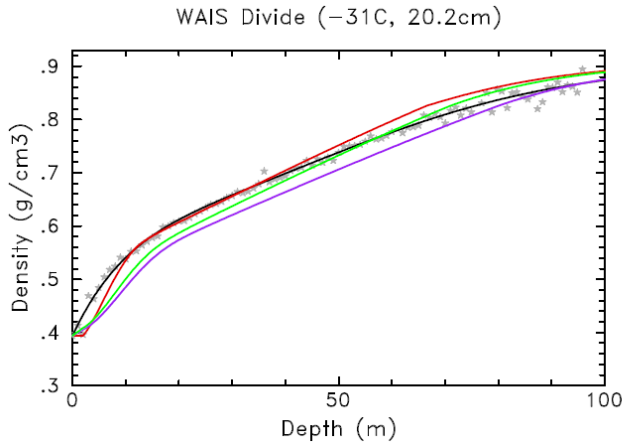
WAIS Divide (−31C, 20.2cm)
Density (g/cm3)
.3
.4
.5
.6
.7
.8
.9
0
50
100
Depth (m)

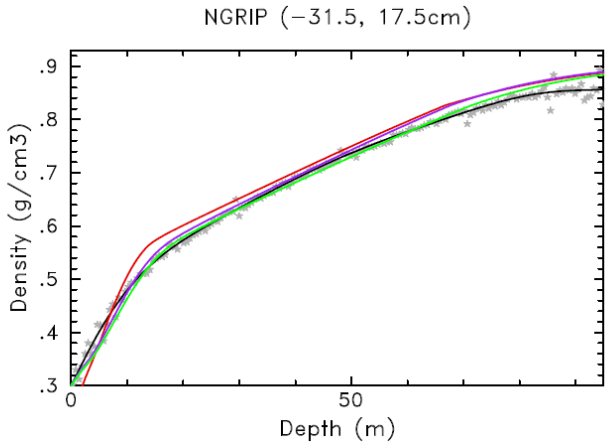
NGRIP (−31.5, 17.5cm)
Density (g/cm3)
.3
.4
.5
.6
.7
.8
.9
0
50
Depth (m)

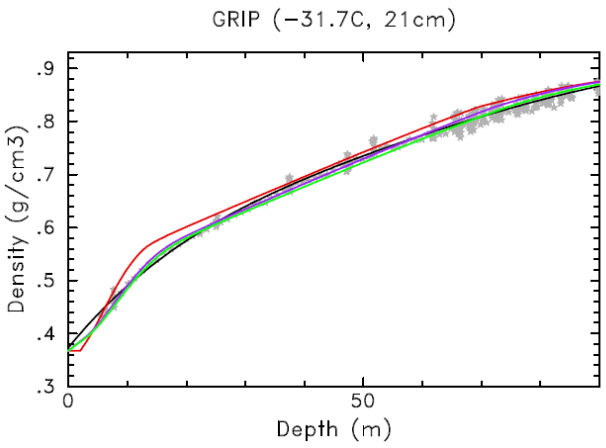
GRIP (−31.7C, 21cm)
Density (g/cm3)
.3
.4
.5
.6
.7
.8
.9
0
50
Depth (m)

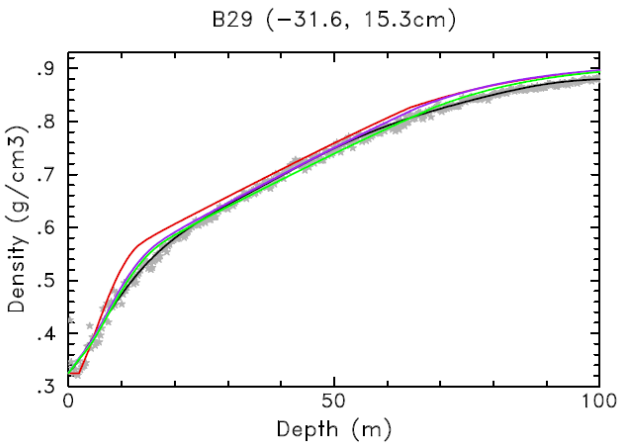
B29 (−31.6, 15.3cm)
Density (g/cm3)
.3
.4
.5
.6
.7
.8
.9
0
50
100
Depth (m)

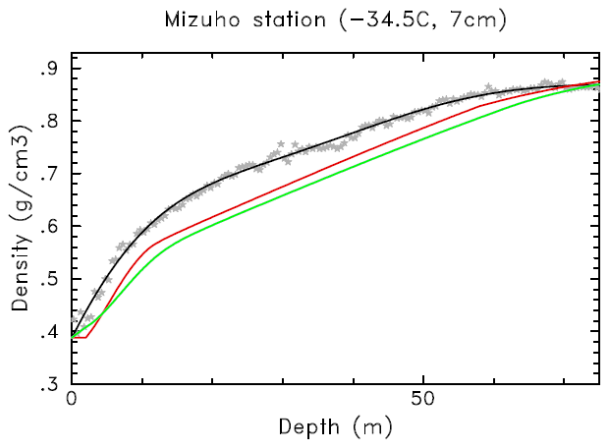
Mizuho station (−34.5C, 7cm)
Density (g/cm3)
.3
.4
.5
.6
.7
.8
.9
0
50
Depth (m)

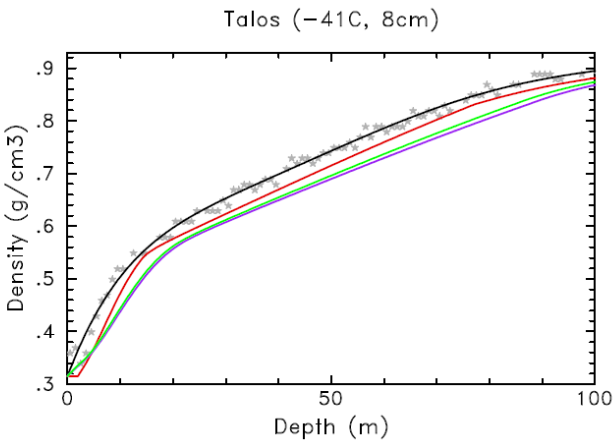
Talos (−41C, 8cm)
Density (g/cm3)
.3
.4
.5
.6
.7
.8
.9
0
50
100
Depth (m)

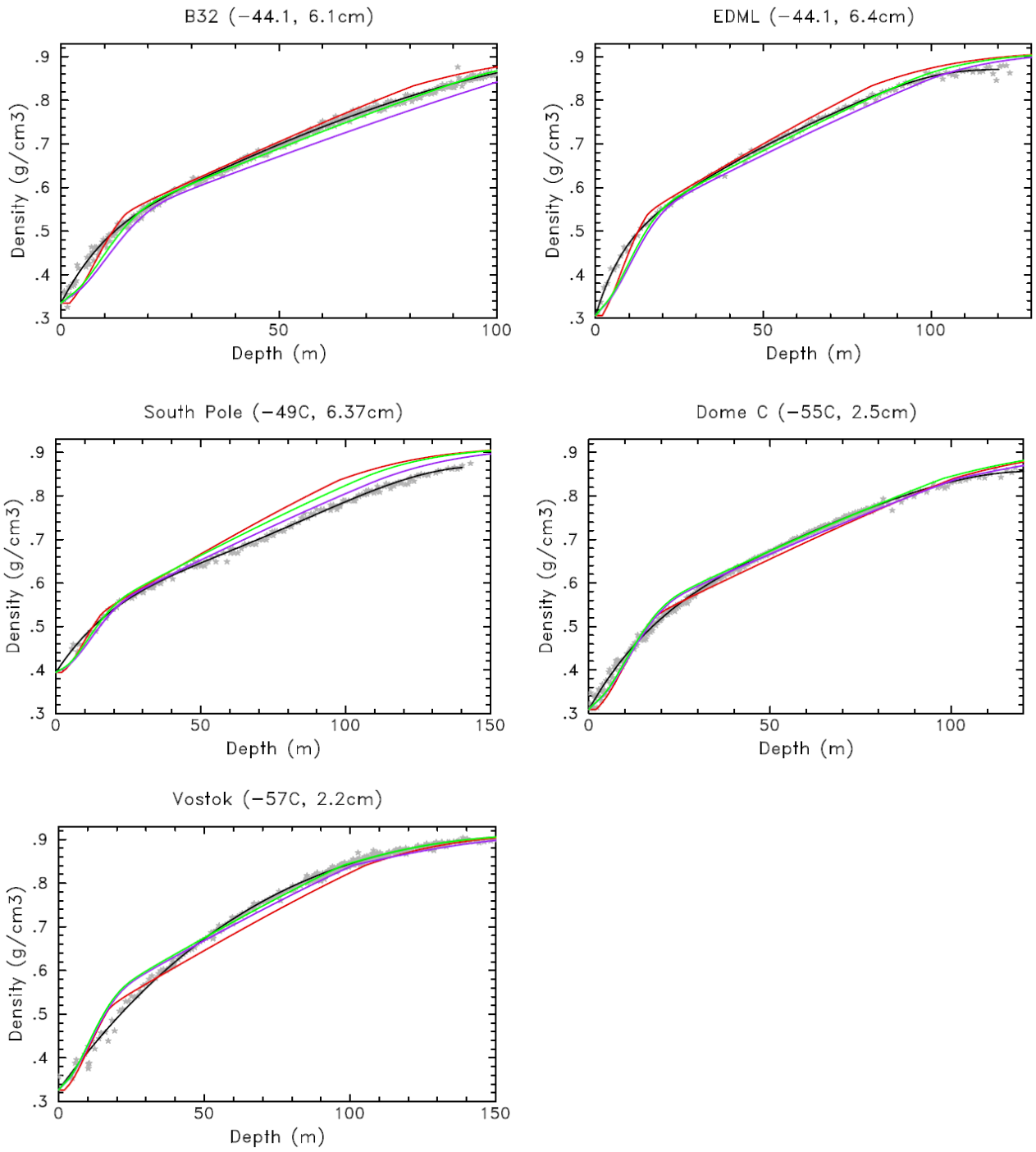

<u>Supplementary Figures S7</u>: Measured and modelled density profiles for 21 sites, the grey stars correspond to the data, the polynomial fit to the data is in black, the density profile simulated with the old version of the LGGE model is in red, the density profile simulated with the new version of the LGGE model is in green and the density profile simulated with the new version of the LGGE model with the dust effect in purple.

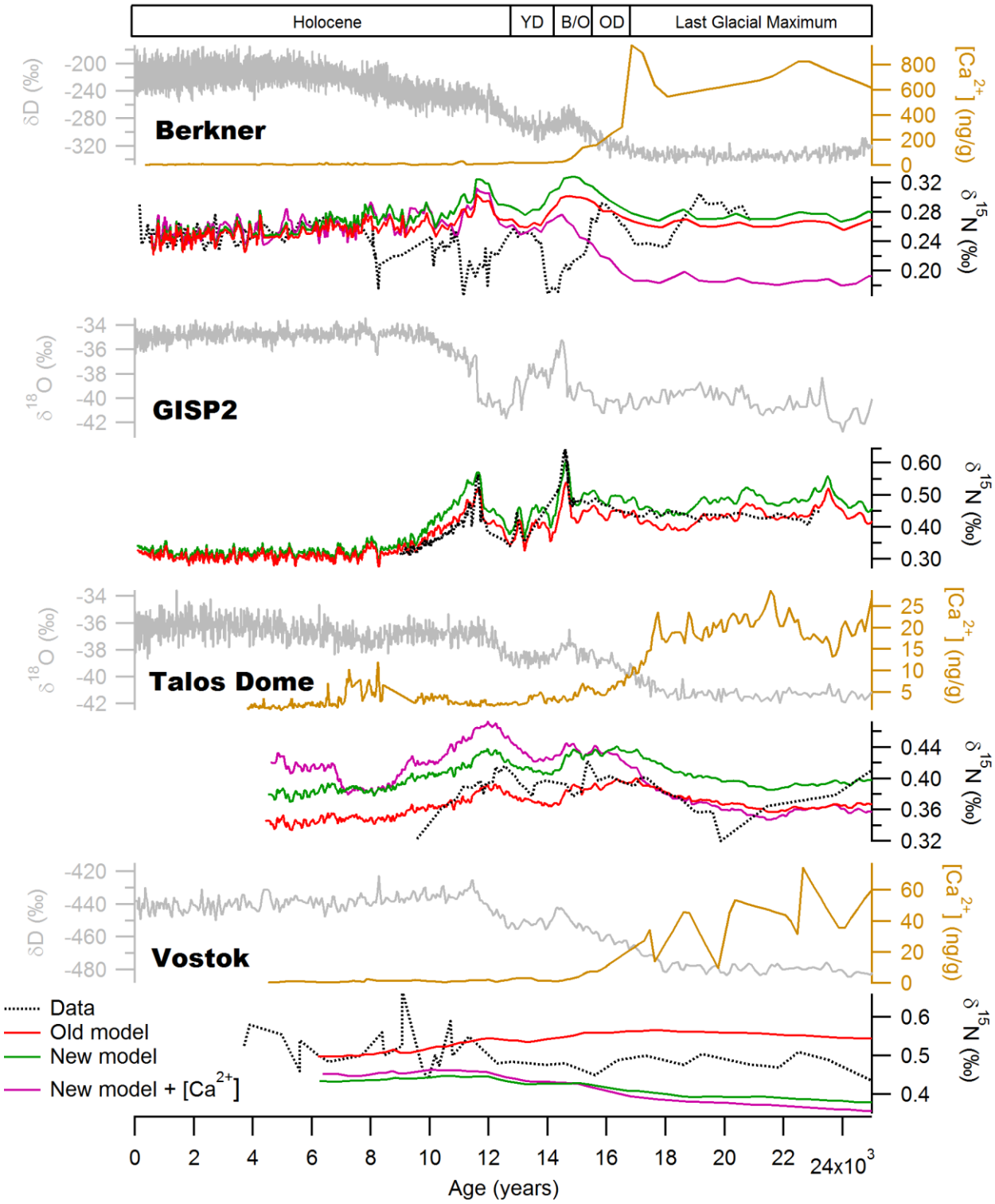

<u>Supplementary Figure S8:</u> Comparison of the measured $\delta^{15}N$ (black) and the modeled $\delta^{15}N$ (old (red), new version (green) and new version with impurity (purple)) of the LGGE model for Berkner, GISP2, Talos Dome and Vostok. The water $\delta^{18}O$ or δD profiles are displayed in grey and the calcium concentration profile in gold.

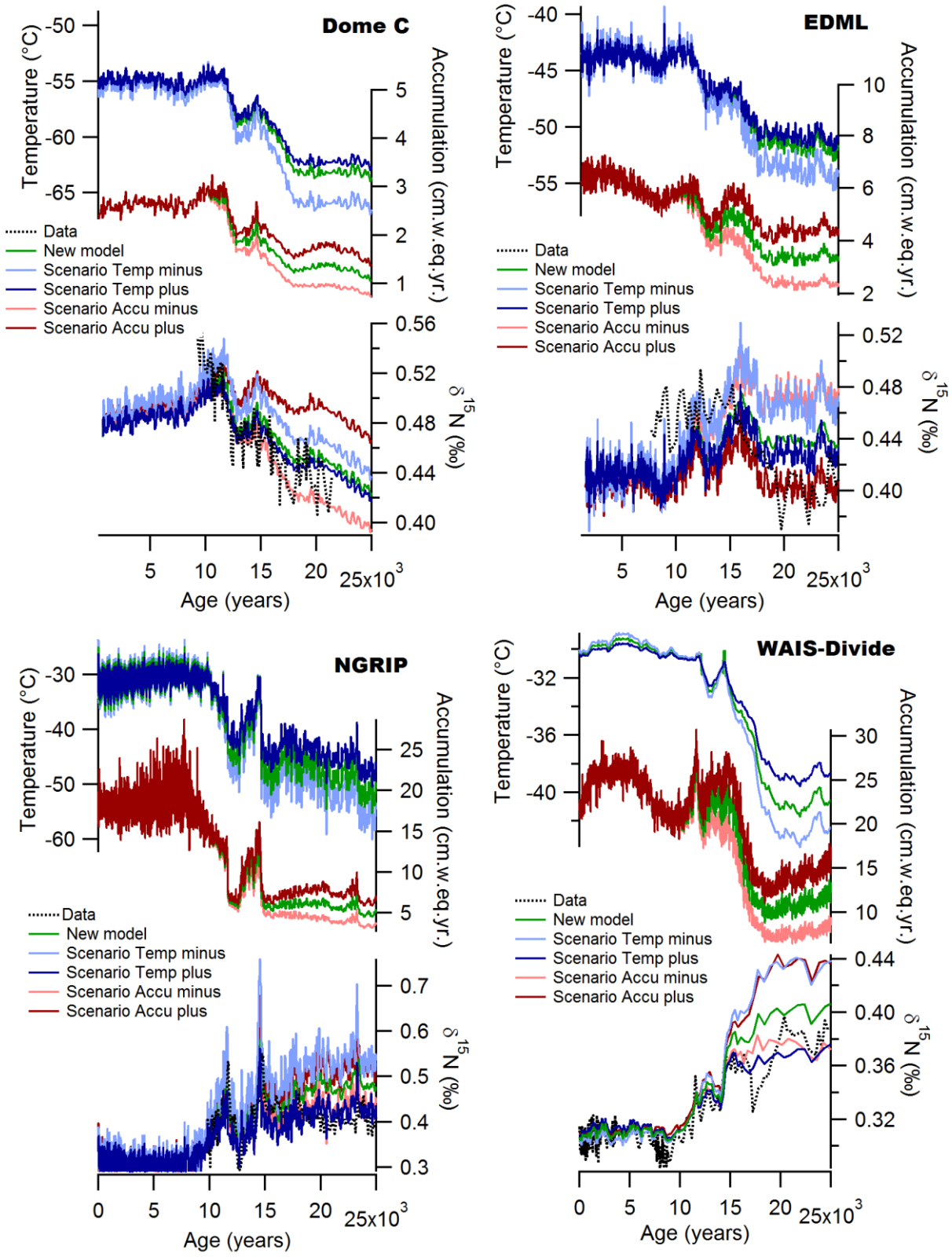

<u>Supplementary Figure S9</u>: Comparison of the measured (black) and modelled $\delta^{15}N$ at Dome C, EDML, NGRIP and WAIS-Divide over the last deglaciation with our new model without impurity effect, using five different temperature and accumulation rate scenarios. The standard scenarios (Table S2) and corresponding $\delta^{15}N$ model outputs are in green. For building the Accu minus/plus and Temp minus/plus scenarios displayed on

the two upper panels for each sites, we took the uncertainties mentioned in the main text: Accu minus correspond to a LGM accumulation rate of -30% (-20%) in Antarctica (Greenland) compared to the standard run; Accu plus corresponds to a LGM accumulation rate of +30% (+20%) in Antarctica (Greenland) compared to the standard run. In Antarctica, Temp plus corresponds to a decrease by 10% of the temperature increase over the last deglaciation (i.e. warmer LGM temperature); Temp minus corresponds to an increase by 30% of the temperature increase over the last deglaciation (i.e. lower LGM temperature). In Greenland, Temp minus and Temp plus are scenarios were the temperature of the LGM is changed by +3 and -3°C.

Within the uncertainty range of the model inputs, it is possible to match the measured $\delta^{15}N$ with the model except for EDML where the modelled $\delta^{15}N$ LGM to EH change is always too small even with the scenario Accu plus. Note that the same figures can be obtained with the old version of the LGGE model with similar amplitude for the differences in simulated LGM $\delta^{15}N$ level between the different scenarios.

Sites	Location (Latitude ; Longitude)	Temperature (°C)	Accumulation (cm.w.eq.yr)	$[Ca^{2+}]$ (ng/g)	Surface density (kg/m^3)	$\sigma_{fit\text{-}data}$ (kg/m^3)	$\sigma_{old\ model\text{-}fit}$ (kg/m^3)	$\sigma_{new\ model\text{-}fit}$ (kg/m^3)	$\sigma_{new\ model\ with\ dust\text{-}fit}$ (kg/m^3)
Dye 3 [1]	65°11'N ; 43°50'W	-18.0	50.0	X	357	13.8	32.7	**30.8**	X
DE08 [2]	66°43'19"S ; 113°11'58"E	-19.0	120.0	X	384.2	10.3	**20.9**	29.8	X
Km105 [4]	67°58'S ; 93°70'E	-24.5	34.1	X	460.5	14.0	**10.7**	21.1	X
Site 2 [5]	76°59'N ; 56°04'W	-25.0	36.0	X	350.1	5.8	**18.3**	19.2	X
Siple Dome [3]	81°39'3"S ; 148°47'66"W	-25.4	10.0	8.0	382.7	8.9	29.4	**13.2**	19.5
D-47 [6]	67°23'S ; 138°43'E	-25.4	25.0	X	377.4	12.5	**15.9**	21.8	X
Byrd [7]	80°S ; 120°W	-28.0	15.6	X	347.1	3.8	**15.9**	18.6	X
NEEM [8]	77.45°N ; 51.06°W	-28.9	20.0	7.4	307.2	8.0	27.2	**13.5**	15.8
Crête (site A) [9]	70°38'5.68"N ; 324°10'48"E	-29.0	28.2	X	321.7	7.0	18.7	**14.0**	X
Km200 [10]	68°15'S ; 94°05'E	-30.5	28.7	X	454.4	10.5	**21.8**	37.7	X
WAIS divide [11]	79°28'S ; 112°05'W	-31.0	20.2	1.58	393.7	8.7	**18.2**	21.3	35.1
Ngrip [12]	75°10'N ; 42°32'W	-31.2	17.5	10.0	299.9	6.9	22.2	**9.9**	13.4
Grip [13]	72°34'N ; 37°37'W	-31.7	21.0	7.8	367.0	6.7	18.9	10.3	**8.8**
B29 [14]	76°00'N ; 43°29'E	-31.6	15.3	9.2	325	10.1	22.7	**7.2**	10.2
Mizuho [15]	70°41'53"S ; 44°19'54"E	-34.5	7.0	X	421	9.8	**50.0**	66.5	X
Talos Dome [16]	72°49'S ; 159°11'E	-41.0	8.0	4.0	315.3	12.1	**29.6**	46.0	51.9
B32 [17]	75°00'S ; 0°00'E	-44.1	6.1	1.7	334.5	6.2	15.6	**13.3**	28.7
EDML [18]	75°S ; 0'04°E	-44.1	6.4	3.0	305.9	5.3	19.4	**16.9**	23.6
South Pole [19]	90°S	-49.0	6.37	2.0	394.4	6.4	35.5	26.7	**15.2**
Dôme C [20]	75°06'S ; 123°21'E	-55.0	2.5	1.8	309.2	6.2	15.3	**11.0**	**11.0**
Vostok [21]	78°28'S ; 106°48'E	-57.0	2.2	1.6	326.5	8.0	28.0	23.5	**23.0**

References below were used for the following data: [a] location, [b] density, [c] temperature, [d] accumulation, [e] calcium concentration
Best efforts were made to find information about the methodologies used for density measurements. The following Greek letters are used to indicate the method used, the use of several letters for the same site implies that several data series were used.

α: volume and weight measurements on whole cores or bags. The precision of such measurements is dependent on the regularity of the core shape.
β: volume and weight measurements in firn, and high precision hydrostatic weighing measurements in ice
γ: volume and weight measurements on machined samples (regular volume, samples are often small)
δ: gamma ray beam attenuation through the ice core (very high resolution)
ε: camera assisted volume measurements, and weight measurements (high resolution)

[1] [a, c, d] Robin, 1983; [b] http://gcmd.nasa.gov/r/d/LSSU_and PSU_Firn_data Spencer et al., 2001
[2] [a, b, c, d] Etheridge and Wookey, 1989; [b] Arnaud et al., 1998, 2000, γ density measurement method
[3] [a, b] https: //nsidc.org/data/waiscores/corec.html, [c] Butler et al., 1999; Jones et al., 2014; Kreutz et al., 1999, 2000, α density measurement method
[4] [a, b, c, d] Salamatin et al., 2009, γ density measurement method
[5] [a, c,] Robin, 1983; [b] http://gcmd.nasa.gov/r/d/LSSU_PSU_Firn_data Spencer et al., 2001 originally from Langway, 1967 with β density measurement method
[6] [a, b, c, d] Arnaud et al., 1998 with β density measurement method
[7] [a, b, c, d] http://gcmd.nasa.gov/r/d/LSSU_PSU_Firn_data Spencer et al., 2001, originally from Gow, 1968 with β density measurement method
[8] [a, b, c] Buizert et al., 2012; [b] Steen-Larsen et al., 2011 ; [e] Gfeller et al., 2014, α density measurement method
[9] [a, b, c, d] http://gcmd.nasa.gov/r/d/LSSU_PSU_Firn_data and Spencer et al., 2001 ; [b]originally from Clausen et al., 1988
[10] [a, b, c, d] Salamatin et al., 2009; [b]Arnaud et al., 1998, γ density measurement method
[11] [a, b, c, d] Fitzpatrick et al., 2014 ; [e] Cole-Dai et al., 2013
[12] [a, c, d] Ngrip community members, 2004, [b] H.C. Steen-Larsen Pers. Comm., [e] Svensson pers. Comm., 2016, α density measurement method
[13] [a, b, c, d] http://gcmd.nasa.gov/r/d/LSSU_PSU_Firn_data and Schwander et al., 1997; [e] Iizuka et al., 2008, α and γ density measurement methods
[14] Freitag et al., 2013; Hörhold et al., 2011, δ density measurement method
[15] [a, c, d] (Nishio et al., 1979) ; [b] (Narita and Maeno, 1978), γ density measurement method
[16] [a, c] www.taldice.org/project/site ; [b] www.taldice.org/data (data from F. Parrenin) ; [d] Stenni et al., 2002 [e] Schüpbach et al., 2013
[17] Freitag et al., 2013; Hörhold et al., 2011, δ density measurement method
[18] [a, b] Kipfstuhl et al., 2009 ; [c] Freitag et al., 2013; [d] Oerter et al., 2004; [e] Fischer et al., 2007, α density measurement method
[19] [a, b, c] http://gcmd.nasa.gov/r/d/LSSU_PSU_Firn_data and Spencer et al., 2001 ; [d] Mosley-Thompson et al., 1995; [e] Ferris et al., 2011
[20] [a, d] Gautier et al., 2016, [b] R. Mulvaney pers. com. and Leduc-Leballeur et al., 2015; [c] Arnaud et al., 2000 ; [e] Lambert et al., 2012, α and ε density measurement methods
[21] [a, c, d] Arnaud et al., 2000 ; [b]http://gcmd.nasa.gov/r/d/LSSU_PSU_Firn_data and Spencer et al., 2001 and J.-M. Barnola, unpublished (using γ density measurement method); [e] De Angelis et al., 1997

Supplementary Table S1: Standard deviation between modeled and measured density profiles for 21 polar sites, for the old LGGE model and the new LGGE model (with three different activation energies in the firn densification module noted "new model" and with three different activation energies depending on Ca^{2+} concentration in the firn densification module noted "new model with dust"). The values in bold indicate the lowest standard deviation between modeled and fitted density profiles for each site.

Sites	Temperature scenario	Accumulation rate scenario	Calcium scenario
NGRIP	Kindler et al., 2014	Bazin et al., 2013	Svensson (comm. pers.) and Seierstad et al., 2014
Dome C	Stenni et al., 2010	Bazin et al., 2013	Fischer et al., 2007 and Lambert et al., 2012
EDML	Stenni et al., 2010	Bazin et al., 2013	Fischer et al., 2007
WAIS-Divide	Buizert et al., 2015 and WAIS Divide Project Members, 2013	Fudge et al., 2016	Buizert et al., 2015
Berkner Island	Capron et al., 2013	Capron et al., 2013	Capron et al., 2013
GISP2	Cuffey and Clow, 1997	Cuffey and Clow 1997	X
Talos Dome	Buiron et al., 2011	Bazin et al., 2013	Schüpbach et al., 2013
Vostok	Cuffey and Vimeux, 2001	Bazin et al., 2013	Legrand et al., 1988

Supplementary Table S2: References of the temperature, accumulation rate and calcium scenarios over the last deglaciation for NGRIP, Dome C, EDML, WAIS-Divide, Berkner Island, GISP2, Talos Dome and Vostok.

EH – LGM (‰)	Dome C	EDML	NGRIP	WAIS-D
Measured	0.1051	0.0538	-0.0986	-0.0780
Old	-0.0404	-0.0446	-0.1080	-0.0639
Old + dust	0.0904	0.0545	-0.0088	-0.0078
New parameterization (Table 1)	0.0519	-0.0313	-0.112	-0.0909
New parameterization + dust	0.0930	0.0651	-0.00937	-0.0129
Test A	-0.0183	-0.0331	-0.0842	-0.0648
Test A + dust	0.0714	0.0474	-0.00282	-0.00658
Test B	-0.0336	-0.0644	-0.147	-0.10
Test B + dust	0.106	0.0604	-0.0272	-0.0225
Test C	0.0265	-0.0463	-0.130	-0.0982
Test C + dust	0.0862	0.0598	-0.0194	-0.0203
New parameterization + dust following Freitag parameterization for the Pimienta – Barnola model	0.0915	0.0646	-0.00717	-0.0092

Supplementary Table S3: Results of the difference between the average of the Early Holocene (EH) and the average of the Last Glacial Maximum (LGM) for the sensitivity tests displayed on Figure 7 for the 4 sites described in the main text.

References

Arnaud, L., Lipenkov, V., Barnola, J.-M., Gay, M. and Duval, P.: Modelling of the densification of polar firn: characterization of the snow-firn transition, in Annals of Glaciology, vol. 26, pp. 39–44., 1998.

Arnaud, L., Barnola, J. M. and Duval, P.: Physical modeling of the densification of snow/firn and ice in, Phys. Ice Ore Rec., 26, 39–44, 2000.

Bazin, L., Landais, A., Lemieux-Dudon, B., Toyé Mahamadou Kele, H., Veres, D., Parrenin, F., Martinerie, P., Ritz, C., Capron, E., Lipenkov, V., Loutre, M. F., Raynaud, D., Vinther, B. M., Svensson, A., Rasmussen, S. O., Severi, M., Blunier, T., Leuenberger, M., Fisher, H., Masson-Delmotte, V., Chappellaz, J. and Wolff, E.: An optimized multi-proxy, multi-site Antarctic ice and gas orbital chronology (AICC2012): 120-800 ka, Clim. Past, 9(4), 1715–1731, 2013.

Buiron, D., Chappellaz, J., Stenni, B., Frezzotti, M., Baumgartner, M., Capron, E., Landais, A., Lemieux-Dudon, B., Masson-Delmotte, V., Montagnat, M., Parrenin, F. and Schilt, A.: TALDICE-1 age scale of the Talos Dome deep ice core, East Antarctica, Clim. Past, 7(1), 1–16, doi:10.5194/cp-7-1-2011, 2011.

Buizert, C., Martinerie, P., Petrenko, V. V., Severinghaus, J. P., Trudinger, C. M., Witrant, E., Rosen, J. L., Orsi, A. J., Rubino, M., Etheridge, D. M., Steele, L. P., Hogan, C., Laube, J. C., Sturges, W. T., Levchenko, V. A., Smith, A. M., Levin, I., Conway, T. J., Dlugokencky, E. J., Lang, P. M., Kawamura, K., Jenk, T. M., White, J. W. C., Sowers, T., Schwander, J. and Blunier, T.: Gas transport in firn: multiple-tracer characterisation and model intercomparison for NEEM, Northern Greenland, Atmospheric Chem. Phys., 12(9), 4259–4277, doi:10.5194/acp-12-4259-2012, 2012.

Buizert, C., Cuffey, K. M., Severinghaus, J. P., Baggenstos, D., Fudge, T. J., Steig, E. J., Markle, B. R., Winstrup, M., Rhodes, R. H., Brook, E. J., Sowers, T. A., Clow, G. D., Cheng, H., Edwards, R. L., Sigl, M., McConnell, J. R. and Taylor, K. C.: The WAIS Divide deep ice core WD2014 chronology-Part 1: Methane synchronization (68–31 ka BP) and the gas age–ice age difference, Clim. Past, 11(2), 153–173, doi:10.5194/cp-11-153-2015, 2015.

Butler, J. H., Battle, M., Bender, M. L., Montzka, S. A., Clarke, A. D., Saltzman, E. S., Sucher, C. M., Severinghaus, J. P. and Elkins, J. W.: A record of atmospheric halocarbons during the twentieth century from polar firn air, Nature, 399(6738), 749–755, 1999.

Capron, E., Landais, A., Buiron, D., Cauquoin, A., Chappellaz, J., Debret, M., Jouzel, J., Leuenberger, M., Martinerie, P., Masson-Delmotte, V., Mulvaney, R., Parrenin, F. and Prié, F.: Glacial–interglacial dynamics of Antarctic firn columns: comparison between simulations and ice core air-δ15N measurements, Clim. Past, 9(3), 983–999, doi:10.5194/cp-9-983-2013, 2013.

Clausen, H. B., Gundestrup, N. S., Johnsen, S. J., Bindschadler, R. and Zwally, J.: Glaciological investigations in the Crete area, central Greenland: A search for a new deep-drilling site, Ann Glaciol, 10, 10–15, 1988.

Cole-Dai, J., Ferris, D. G., Lanciki, A. L., Savarino, J., Thiemens, M. H. and McConnell, J. R.: Two likely stratospheric volcanic eruptions in the 1450s CE found in a bipolar, subannually dated 800 year ice core record, J. Geophys. Res. Atmospheres, 118(14), 7459–7466, 2013.

Cuffey, K. M. and Clow, G. D.: Temperature, accumulation, and ice sheet elevation in central Greenland through the last deglacial transition, J. Geophys. Res. Oceans, 102(C12), 26383–26396, 1997.

Cuffey, K. M. and Vimeux, F.: Covariation of carbon dioxide and temperature from the Vostok ice core after deuterium-excess correction, Nature, 523–526, 2001.

De Angelis, M., Steffensen, J. P., Legrand, M., Clausen, H. and Hammer, C.: Primary aerosol (sea salt and soil dust) deposited in Greenland ice during the last climatic cycle: Comparison with east Antarctic records, J. Geophys. Res. Oceans, 102(C12), 26681–26698, 1997.

Etheridge, D. M. and Wookey, C. W.: Ice core drilling at a high accumulation area of Law Dome, Antarctica. 1987, Ice Core Drill., 10–14, 1988.

Ferris, D. G., Cole-Dai, J., Reyes, A. R. and Budner, D. M.: South Pole ice core record of explosive volcanic eruptions in the first and second millennia A.D. and evidence of a large eruption in the tropics around 535 A.D., J. Geophys. Res., 116(D17), doi:10.1029/2011JD015916, 2011.

Fischer, H., Fundel, F., Ruth, U., Twarloh, B., Wegner, A., Udisti, R., Becagli, S., Castellano, E., Morganti, A., Severi, M., Wolff, E., Littot, G., Röthlisberger, R., Mulvaney, R., Hutterli, M. A., Kaufmann, P., Federer, U., Lambert, F., Bigler, M., Hansson, M., Jonsell, U., de Angelis, M., Boutron, C., Siggaard-Andersen, M.-L., Steffensen, J. P., Barbante, C., Gaspari, V., Gabrielli, P. and Wagenbach, D.: Reconstruction of millennial changes in dust emission, transport and regional sea ice coverage using the deep EPICA ice cores from the Atlantic and Indian Ocean sector of Antarctica, Earth Planet. Sci. Lett., 260(1–2), 340–354, doi:10.1016/j.epsl.2007.06.014, 2007.

Fitzpatrick, J. J., Voigt, D. E., Fegyveresi, J. M., Stevens, N. T., Spencer, M. K., Cole-Dai, J., Alley, R. B., Jardine, G. E., Cravens, E. D., Wilen, L. A., Fudge, T. J. and McConnell, J. R.: Physical properties of the WAIS Divide ice core, J. Glaciol., 60(224), 1181–1198, doi:10.3189/2014JoG14J100, 2014.

Freitag, J., Kipfstuhl, S., Laepple, T. and Wilhelms, F.: Impurity-controlled densification: a new model for stratified polar firn, J. Glaciol., 59(218), 1163–1169, doi:10.3189/2013JoG13J042, 2013.

Fudge, T. J., Markle, B. R., Cuffey, K. M., Buizert, C., Taylor, K. C., Steig, E. J., Waddington, E. D., Conway, H. and Koutnik, M.: Variable relationship between accumulation and temperature in West Antarctica for the past 31,000 years: wdc temperature and accumulation, Geophys. Res. Lett., 43(8), 3795–3803, doi:10.1002/2016GL068356, 2016.

Gautier, E., Savarino, J., Erbland, J., Lanciki, A. and Possenti, P.: Variability of sulfate signal in ice core records based on five replicate cores, Clim. Past, 12(1), 103–113, doi:10.5194/cp-12-103-2016, 2016.

Gfeller, G., Fischer, H., Bigler, M., Schüpbach, S., Leuenberger, D. and Mini, O.: Representativeness and seasonality of major ion records derived from NEEM firn cores, The Cryosphere, 8(5), 1855–1870, doi:10.5194/tc-8-1855-2014, 2014.

Goujon, C., Barnola, J.-M. and Ritz, C.: Modeling the densification of polar firn including heat diffusion: Application to close-off characteristics and gas isotopic fractionation for Antarctica and Greenland sites, J. Geophys. Res. Atmospheres, 108(D24), 2003.

Gow, A. J.: Deep core studies of the accumulation and densification of snow at Byrd station and Little America V, Antarctica, CRREL., 1968.

Hörhold, M. W., Kipfstuhl, S., Wilhelms, F., Freitag, J. and Frenzel, A.: The densification of layered polar firn, J. Geophys. Res. Earth Surf., 116(F1), 2011.

Iizuka, Y., Horikawa, S., Sakurai, T., Johnson, S., Dahl-Jensen, D., Steffensen, J. P. and Hondoh, T.: A relationship between ion balance and the chemical compounds of salt inclusions found in the Greenland Ice Core Project and Dome Fuji ice cores, J. Geophys. Res., 113(D7), doi:10.1029/2007JD009018, 2008.

Jones, T. R., White, J. W. C. and Popp, T.: Siple Dome shallow ice cores: a study in coastal dome microclimatology, Clim. Past, 10(3), 1253–1267, doi:10.5194/cp-10-1253-2014, 2014.

Kindler, P., Guillevic, M., Baumgartner, M., Schwander, J., Landais, A., Leuenberger, M., Spahni, R., Capron, E. and Chappellaz, J.: Temperature reconstruction from 10 to 120 kyr b2k from the NGRIP ice core, Clim. Past, 10(2), 887–902, doi:10.5194/cp-10-887-2014, 2014.

Kipfstuhl, S., Faria, S. H., Azuma, N., Freitag, J., Hamann, I., Kaufmann, P., Miller, H., Weiler, K. and Wilhelms, F.: Evidence of dynamic recrystallization in polar firn, J. Geophys. Res., 114(B5), doi:10.1029/2008JB005583, 2009.

Kreutz, K. J., Mayewski, P. A., Twickler, M. S., Whitlow, S. I., White, J. W. C., Shuman, C. A., Raymond, C. F., Conway, H. and McConnell, J. R.: Seasonal variations of glaciochemical, isotopic and stratigraphic properties in Siple Dome (Antarctica) surface snow, Ann. Glaciol., 29(1), 38–44, 1999.

Kreutz, K. J., Mayewski, P. A., Meeker, L. D., Twickler, M. S. and Whitlow, S. I.: The effect of spatial and temporal accumulation rate variability in West Antarctica on soluble ion deposition, Geophys. Res. Lett., 27(16), 2517, 2000.

Lambert, F., Bigler, M., Steffensen, J. P., Hutterli, M. and Fischer, H.: Centennial mineral dust variability in high-resolution ice core data from Dome C, Antarctica, Clim. Past, 8(2), 609–623, doi:10.5194/cp-8-609-2012, 2012.

Langway, C. C. J.: Stratigraphic analysis of a deep ice core from Greenland, CRREL Res. Rep. 77, pp 130, 1967.

Leduc-Leballeur, M., Picard, G., Mialon, A., Arnaud, L., Lefebvre, E., Possenti, P. and Kerr, Y.: Modeling L-band brightness temperature at Dome C in Antarctica and comparison with SMOS observations, IEEE Trans. Geosci. Remote Sens., 53(7), 4022–4032, 2015.

Legrand, M. R., Lorius, C., Barkov, N. I. and Petrov, V. N.: Vostok (Antarctica) ice core: atmospheric chemistry changes over the last climatic cycle (160,000 years), Atmospheric Environ. 1967, 22(2), 317–331, 1988.

Mosley-Thompson, E., Thompson, L. G., Paskievitch, J. F., Pourchet, M., Gow, A. J., Davis, M. E. and Kleinman, J.: Recent increase in South Pole snow accumulation, Ann. Glaciol., 21(1), 131–138, 1995.

Narita, H. and Maeno, N.: II. Compiled Density Data from Cores Drilled at Mizuho Station (Appendix: Miscellaneous Compiled Data), Mem. Natl. Inst. Polar Res. Spec. Issue, 10, 136–158, 1978.

Ngrip community members: High-resolution record of Northern Hemisphere climate extending into the last interglacial period, Nature, 431(7005), 147–151, 2004.

Nishio, F., Fuji, Y. and Kusunoki, K.: Measured and computed temperature profiles at Mizuho station, East Antarctica, Sea Level Lee Clim. Change, 239–246, 1979.

Oerter, H., Graf, W., Meyer, H. and Wilhelms, F.: The EPICA ice core from Dronning Maud Land: first results from stable-isotope measurements, Ann. Glaciol., 39(1), 307–312, 2004.

Robin, G. de Q.: Profile data, Greenland region, Clim. Rec. Polar Ice Sheets Camb. Univ. Press Camb., 98–111, 1983.

Salamatin, A. N., Lipenkov, V. Y., Barnola, J. M., Hori, A., Duval, P. and Hondoh, T.: Snow/firn densification in polar ice sheets, Phys. Ice Core Rec. - II, 68(Supplement), 195–222, 2009.

Schüpbach, S., Federer, U., Kaufmann, P. R., Albani, S., Barbante, C., Stocker, T. F. and Fischer, H.: High-resolution mineral dust and sea ice proxy records from the Talos Dome ice core, Clim. Past, 9(6), 2789–2807, doi:10.5194/cp-9-2789-2013, 2013.

Schwander, J., Sowers, T., Barnola, J.-M., Blunier, T., Fuchs, A. and Malaizé, B.: Age scale of the air in the summit ice: Implication for glacial-interglacial temperature change, J. Geophys. Res. Atmospheres, 102(D16), 19483–19493, 1997.

Seierstad, I. K., Abbott, P. M., Bigler, M., Blunier, T., Bourne, A. J., Brook, E., Buchardt, S. L., Buizert, C., Clausen, H. B., Cook, E., Dahl-Jensen, D., Davies, S. M., Guillevic, M., Johnsen, S. J., Pedersen, D. S., Popp, T. J., Rasmussen, S. O., Severinghaus, J. P., Svensson, A. and Vinther, B. M.: Consistently dated records from the Greenland GRIP, GISP2 and NGRIP ice cores for the past 104 ka reveal regional millennial-scale δ18O gradients with possible Heinrich event imprint, Quat. Sci. Rev., 106, 29–46, doi:10.1016/j.quascirev.2014.10.032, 2014.

Spencer, M. K., Alley, R. B. and Creyts, T. T.: Preliminary firn-densification model with 38-site dataset, J. Glaciol., 47(159), 671–676, 2001.

Steen-Larsen, H. C., Masson-Delmotte, V., Sjolte, J., Johnsen, S. J., Vinther, B. M., Bréon, F.-M., Clausen, H. B., Dahl-Jensen, D., Falourd, S., Fettweis, X., Gallée, H., Jouzel, J., Kageyama, M., Lerche, H., Minster, B., Picard, G., Punge, H. J., Risi, C., Salas, D., Schwander, J., Steffen, K., Sveinbjörnsdóttir, A. E., Svensson, A. and White, J.: Understanding the climatic signal in the water stable isotope records from the NEEM shallow firn/ice cores in northwest Greenland, J. Geophys. Res., 116(D6), doi:10.1029/2010JD014311, 2011.

Stenni, B., Proposito, M., Gragnani, R., Flora, O., Jouzel, J., Falourd, S. and Frezzotti, M.: Eight centuries of volcanic signal and climate change at Talos Dome (East Antarctica), J. Geophys. Res. Atmospheres, 107(D9), 2002.

Stenni, B., Masson-Delmotte, V., Selmo, E., Oerter, H., Meyer, H., Röthlisberger, R., Jouzel, J., Cattani, O., Falourd, S., Fischer, H., Hoffmann, G., Iacumin, P., Johnsen, S. J., Minster, B. and Udisti, R.: The deuterium excess records of EPICA Dome C and Dronning Maud Land ice cores (East Antarctica), Quat. Sci. Rev., 29(1–2), 146–159, doi:10.1016/j.quascirev.2009.10.009, 2010.

WAIS Divide Project Members: Onset of deglacial warming in West Antarctica driven by local orbital forcing, Nature, 500(7463), 440–444, doi:10.1038/nature12376, 2013.

Witrant, E., Martinerie, P., Hogan, C., Laube, J. C., Kawamura, K., Capron, E., Montzka, S. A., Dlugokencky, E. J., Etheridge, D., Blunier, T. and Sturges, W. T.: A new multi-gas constrained model of trace gas non-homogeneous transport in firn: evaluation and behaviour at eleven polar sites, Atmospheric Chem. Phys., 12(23), 11465–11483, doi:10.5194/acp-12-11465-2012, 2012.